DXAFS 分光法による種々の TiO_2 上への Rh 金属粒子の光電析のその観察
Effect of a Crystalline Phase of a TiO_2 photocatalyst on the Photodeposition of Rh Metal Nanoparticles

大山順也（D3），山本旭，寺村謙太郎，宍戸哲也，田中庸裕
Junya Ohyama, Akira Yamamoto, Teramura Kentaro, Tetsuya Shishido, Tsunehiro Tanaka

京都大学研究科分子工学専攻
Department of Molecular Engineering, Graduate School of Engineering, Kyoto University

Abstract

Effect of a crystalline phase of TiO_2 is investigated in the photodeposition processes of Rh metal nanoparticles on some TiO_2 photocatalysts having anatase and rutile phase by means of in situ time-resolved energy dispersive X-ray absorption fine structure spectroscopy (DXAFS). The important factor was not its crystallite size nor its specific surface area but the crystalline phase. In situ time-resolved DXAFS analysis clarified that the Rh metal nanoparticles with a uniform size appear on both anatase and rutile phases of TiO_2, whereas the appearance rate of Rh metal nanoparticles decreases with the photoirradiation time only on the rutile phase of TiO_2. These results suggest that the crystalline phase of TiO_2 has an effect on rates of formation of $TiO_{2-\delta}$ and reduction of Rh^{3+} ions to Rh metal nanoparticles on $TiO_{2-\delta}$.

Introduction

It has widely been recognized that the photodeposition, which Bard et al. have reported in 1978,[1] is a very valuable method to recover of noble metals, to remove metal cations from aqueous effluent, and to prepare metal−supported catalysts and metal-promoted photocatalysts.[2-4] Photoexcited electrons in a photocatalyst reduce metal cations which exhibits more positive redox potential than the conduction-band level of the photocatalyst. The simultaneously generated holes in the valence band are consumed to react with a sacrificial reagent such as alcohol, aldehyde, or carboxylic acid which promote photodeposition smoothly.[1,3] In the several studies, we can find that the photodeposited metal species modify specific sites on a photocatalyst, for example, an edge or plane of a photocatalyst crystallite.[5] Interestingly, the morphology of the resulting metal nanoparticles greatly varies among the kinds of photocatalyst. These phenomena inspire us to study the systematic kinetics and mechanism for the formation of nanoparticles as well as the structure of resulting metal species. X-ray absorption fine structure (XAFS) spectroscopy is a powerful method to analyze photodeposition process. Fernandez et al. have observed the photodeposition of Au nanoparticles by an in situ XAFS measurement, where the suspension composed of an Au precursor and TiO_2 was pumped out from the photochemical reactor to the XAFS measurement cell under photoirradiation.[6] We have also successfully observed the photodeposition process of Rh metal nanoparticles on TiO_2 using in situ time-resolved energy dispersive X-ray absorption fine structure spectroscopy (DXAFS), and proposed unique particle-formation mechanism that Rh metal nanoparticles with a uniform size constantly appear one after another on the surface of TiO_2.[7,8]

Very recently, we reported that photodeposited Rh and Pt metal nanoparticles on TiO_2 (JRC-TIO-8, anatase) were modified with $TiO_{2-\delta}$ which is well-known as a key species in the strong metal-support interaction (SMSI).[9] Generally, the SMSI can be observed when group VIII noble metals (e.g., Pt, Rh, Pd, and Ir) on reducible oxide supports (e.g., TiO_2 and Nb_2O_5) are treated with H_2 at high temperature and causes the modification of metal nanoparticles with reduced supports (e.g., $TiO_{2-\delta}$) generated by H_2 treatment. It is both interesting and incredible that the SMSI take places under photoirradiation at room temperature as well as by H_2 treatment at high temperature. Most probably, $TiO_{2-\delta}$ generated by the photoirradiation of TiO_2 cause the modification and the disorganized structure of Rh and Pt metal

Table 1. Properties of various TiO_2 photocatalysts.

	Crystalline phase	Crystallite size (nm)	Specific surface area ($m^2 g^{-1}$)
JRC-TIO-8	Anatase	15.5	91.0
JRC-TIO-1	Anatase	18.7	75.1
JRC-TIO-10	Anatase	16.9	128
JRC-TIO-3	Rutile	21.9	47.1
JRC-TIO-6	Rutile	24.0	50.5

nanoparticles. Amount, type and property of $TiO_{2-\delta}$, therefore, may have an effect on the SMSI in the photodeposition process. Li et al. reported that the SMSI occurs by H_2 reduction at lower temperature on anatase TiO_2 than on rutile.[10] In this study, we investigated the photodeposition processes of Rh metal nanoparticles on TiO_2 photocatalysts having anatase and rutile phases, and their structure by means of in situ time-resolved DXAFS spectroscopy.

Experimental Section

TiO_2 samples used in this study (JRC-TIO-1, 3, 6, 8, and 10) were kindly supplied from the Japan Catalysis Society. All the samples were calcined in air at 673 K for 3 h before use. Crystalline phase of each TiO_2 was determined by X-ray diffraction technique (XRD). The crystallite size was estimated by the use of the Scherrer's equation. The specific surface area of sample was determined using N_2 adsorption isotherm at 77 K. Table 1 lists crystalline phases, surface areas, and crystallite sizes of TiO_2 used in this study. In this paper, for simplicity, we denote the phase and the catalyst like **N-X** where **N** is the catalyst name JRC-TIO-**N**, and **X** is **A** or **R** meaning anatase or rutile, respectively; i.e., JRC-TIO-8 (anatase) to **8-A** and JRC-TIO-3 (rutile) to **3-R**.

The photodeposition of Rh nanoparticles on TiO_2 was carried out in a closed batch system. As a typical photodeposition method, 500 mg of TiO_2 was suspended in 3.2 mL of methanol in a batch reactor made of Pyrex glass with a flat ceiling window for irradiation, followed by the addition of 0.8 mL of a $RhCl_3$ (Wako Pure Chemical Industries, Ltd.) aqueous solution (0.076 mmol of Rh). The suspension was irradiated with a 200 W Hg-Xe lamp equipped

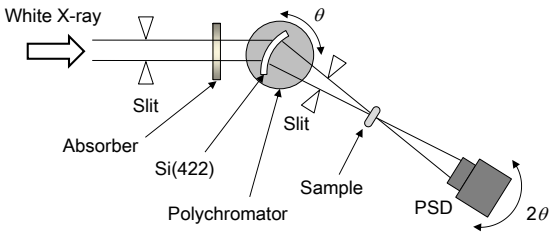

Scheme 1. Main equipment of the DXAFS spectroscopy system at the BL28B2 beamline

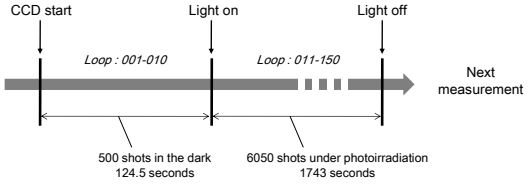

Scheme 2. Timetable of the DXAFS analysis in this study

with fiber optics, a collective lens, and a mirror (San-Ei Electric Co., Ltd., UVF-204S type C) after N_2 bubbling for 10 min. Then the suspension was filtered, and the residual powder was washed with 100 mL of purified water and was placed in an oven at 353 K.

In situ time-resolved DXAFS measurements at the Rh-K edge (~23.2 keV) were performed on the BL28B2 beamline at the SPring-8. The DXAFS measurement system consists of a polychromator set to a Laue configuration with a Si (422) net plane and a position-sensitive detector (PSD) mounted on a θ - 2θ diffractometer as shown in Scheme 1. The X-ray energy was calibrated by the spectrum of a Rh foil. The above-mentioned Pyrex reactor with the suspension was set at the X-ray focal spot. Light irradiation of the reactor was synchronized with exposure to X-rays. Scheme 2 shows the timetable of the DXAFS measurement in this study. The exposure time of the PSD was 249 ms. Fifty shots were accumulated; 12.45 s per a spectrum. We programmed the collection of 500 snapshot spectra (124.5 s) in the dark and then 7000 snapshot spectra (1743 s) under photoirradiation consecutively. The measurement program was repeated four times to obtain the spectral change at 116.2 min under photoirradiation. Analysis of XAFS spectra was performed using the REX2000 program (version 2.5.9, Rigaku Corp.). The k^3-weighted EXAFS oscillation in the range of 2.78-10.7 Å was Fourier-transformed.

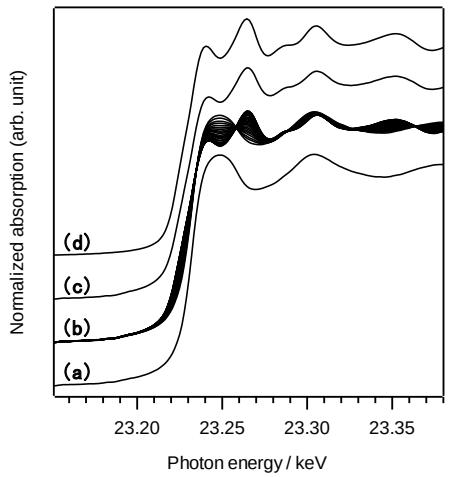

Figure 1. XANES spectra at the Rh-K edge of reference samples and the suspension consisting of a $RhCl_3$ methanol-aqueous solution and **3-R**: (a) before irradiation, (b) under irradiation, (c) after irradiation for 116 min, and (d) Rh foil.

Results and Discussion

Figure 1 shows a series of Rh-K edge XANES spectra of the suspension consisting of an $RhCl_3$ methanol aqueous solution and **3-R** under photoirradiation. The edge energy of XANES shifted to lower photon energy with the elongation of photoirradiation time. The XANES spectrum after 116 min of photoirradiation was almost identical to that of the Rh foil. This result indicates that Rh^{3+} ions are reduced to Rh^0 metals by photoirradiation. It should also be mentioned that there is no change in the spectrum from $RhCl_3$ without TiO_2 or photoirradiation. The XANES spectral change corresponding to the reduction of Rh^{3+} ions to Rh^0 metals exhibits the isosbestic points, which indicates that Rh^{3+} ions are reduced to Rh^0 metals without any intermediates within the measurable time. All the Rh-K edge XANES spectra can be represented with the linear combination of the two XANES spectra; one is that of Rh^{3+} ions in the initial state; and the other is that of Rh^0 metals in the final state. The least-squares fitting of each XANES spectrum with the linear combination allowed us to obtain the fractions of the Rh^0 metals and Rh^{3+} ions using **3-R** and **8-A** as shown in **Figure 2**. The fraction of Rh^0 metals increased with the photoirradiation time in both cases. In the case of **3-R**, the rate of an increase in Rh^0 metals decelerated with the photoirradiation time and the fraction of Rh^0 metals was saturated after 90 min. The deceleration of increasing rate of Rh^0 metals means that the rate of reduction of Rh^{3+} ions to Rh^0 metals was lowered with photoirradiation time. In the case of **8-A**, the Rh^0 metal fraction linearly increased with photoirradiation time and became constant at 75 min, which indicates that the Rh^{3+} ions are reduced to Rh^0 metals at a constant rate. On the other hand, the behavior of reduction of Rh^{3+} ions to Rh^0 metals on **3-R** is different from that on **8-A**. **Figure 3** shows the dependence of the fraction of Rh^0 metals on photoirradiation time in the case of (a) rutile phase (**3-R** and **6-R**) and (b) anatase phase (**1-A**, **8-A**, and **10-A**) of TiO_2. When the rutile were used, the reduction rate of Rh^{3+} ions decreased with photoirradiation time as represented by the case of **3-R**. Whereas, the reduction rate of Rh^{3+} ions on the anatase phase was constant with photoirradiation time as represented by the case of **8-A**. The behavior of reduction of Rh^{3+} ions to Rh^0 metals on the rutile is different from that on the anatase. These results strongly suggest that the crystalline phase of TiO_2 exerts an influence on the formation rate of Rh^0 metals for the photodeposition

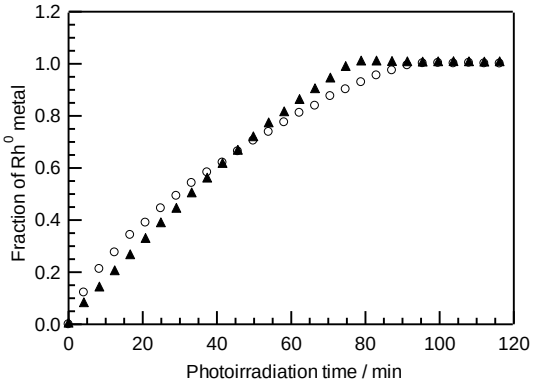

Figure 2. Dependence of the fraction of Rh^0 metals in the case of **3-R** (○) and **8-A** (▲).

Figure 4 shows a series of Fourier transforms (FTs) of k^3-weighted Rh-K edge EXAFS spectra of Rh species for photodeposition on **3-R**. The peak located at 1.73 Å is assignable to the mixture of Rh-Cl and Rh-O scattering of $RhCl_3$ in solution and adsorbed on TiO_2. The height of the peak at 1.73 Å decreased with increasing photoirradiation time, and an alternative peak appeared at 2.45 Å. The peak at 2.45 Å is assigned to the Rh-Rh scattering of Rh^0 metal nanoparticles generated by

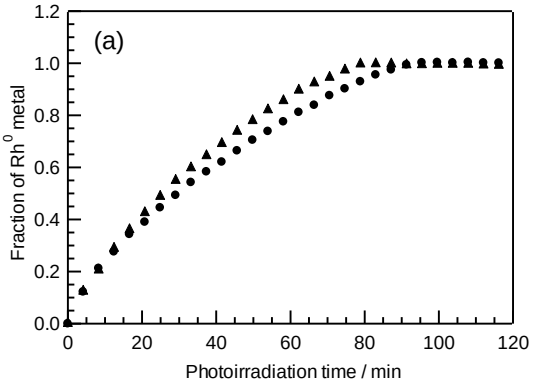

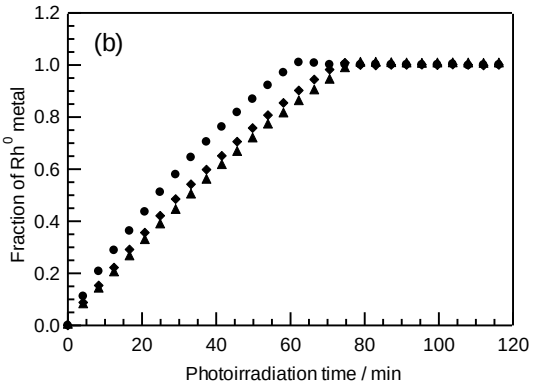

Figure 3. Dependence of the fraction of Rh^0 metal in the case of (a) TiO_2 (rutile), **3-R** (●), **6-R** (▲) and (b) TiO_2 (anatase), **1-A** (●), **8-A** (▲), **10-A** (♦).

photoirradiation. The peak height at 2.45 Å rose with photoirradiation time and saturated at 90 min. **Figure 5** demonstrates the photoirradiation time dependence of the C.N.(Rh-Rh) in the case of **3-R** and **8-A**. The coordination number of Rh-Rh bonds (C.N.(Rh-Rh)) of each sample was estimated from the peak height of FT of EXAFS by using the ratio of C.N.(Rh-Rh) of Rh foil (12) to the peak height (24). In the case of **3-R**, the increase in the amount of change of C.N.(Rh-Rh) value was getting sluggish with the photoirradiation time and the value was saturated after 90 min of photoirradiation. In the case of **8-A**, the C.N.(Rh-Rh) increased proportionally to the photoirradiation time, and attained to 10 after 75 min of photoirradiation. In both the cases, the behaviors of the C.N.(Rh-Rh) change perfectly corresponded to those of the fraction of Rh^0 metals estimated by analyses of XANES spectra.

The C.N.(Rh-Rh) estimated by EXAFS analysis are the average for all the existing Rh elements. Therefore, the C.N.(Rh-Rh) is given by

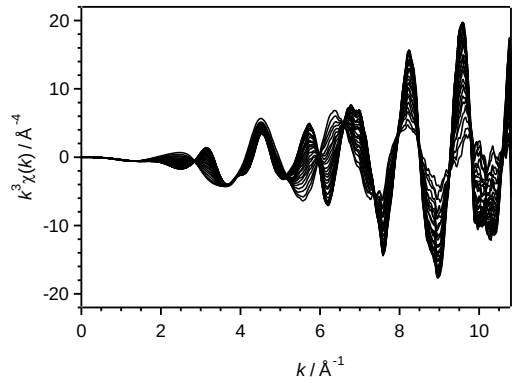

Figure 4. Series of k^3-weighted Rh-K edge EXAFS spectra of Rh species during the photodeposition on **3-R**.

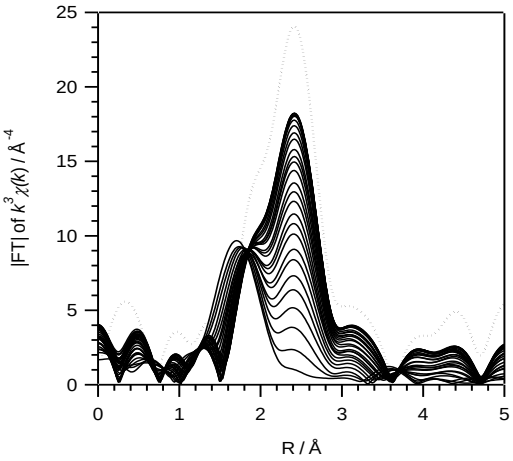

Figure 5. Series of the FT of k^3-weighted Rh-K edge EXAFS spectra of Rh species during the photodeposition in the case of **3-R**.

$$C.N.(Rh\text{-}Rh) = C.N._{Rh0}X_{Rh0} \qquad (1)$$

where the $C.N._{Rh0}$ is the C.N. of Rh^0 in the nanoparticles and the X_{Rh0} the fraction of Rh^0 in the suspension. Thus, the $C.N._{Rh0}$ was calculated by the following equation.

$$C.N._{Rh0} = C.N.(Rh\text{-}Rh)/X_{Rh0} \qquad (2)$$

By using equation (2), the photoirradiation time dependence of the $C.N._{Rh0}$ in the case of **3-R** and **8-A** is calculated from the Rh^0 metal fraction and the C.N.(Rh-Rh) shown in **Figure 2** and **Figure 5**. As a result, the $C.N._{Rh0}$ on **3-R** and **8-A** were constant with photoirradiation time as shown in **Figure 6**. This result indicates that Rh metal nanoparticles with a uniform size appear one after another on both kinds of TiO_2 during the photodeposition and the sizes never grow up. It is concluded that the difference in variation of

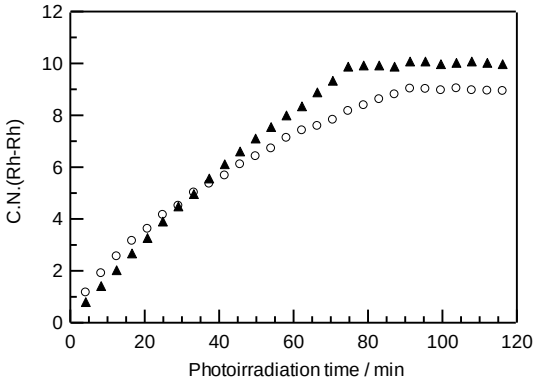

Figure 6. Photoirradiation time dependence of the C.N.(Rh-Rh) in the case of **3-R** (○) and **8-A** (▲).

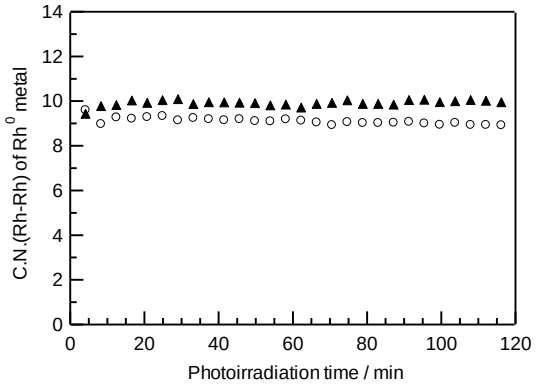

Figure 7. Photoirradiation time dependence of the C.N.(Rh-Rh) of Rh^0 metal in the case of **3-R** (○) and **8-A** (▲).

C.N.(Rh-Rh) between **3-R** and **8-A** resulted from the difference in the appearance rate of Rh metal nanoparticles. In other words, the Rh metal nanoparticles with a uniform size appear both on the anatase and rutile, whereas the appearance rate decreases with the photoirradiation time only on the-rutile.

As mentioned above, the appearance rate of Rh metal nanoparticles is constant using anatase phase of TiO_2 and decreases with the photoirradiation time using the rutile, although the Rh metal nanoparticles with a uniform size constantly appear on both the anatase and the rutile. This means that the active sites for reduction of Rh^{3+} ions to Rh metal nanoparticles with the uniform size decreases in the case of the rutile as the photodeposition proceeds. The active sites for the reduction of Rh^{3+} ions on the rutile , which is Ti^{3+} sites in $TiO_{2-\delta}$ generated by photoirradiation (and those in defect site inherent in TiO_2 powder)[11,12], is masked by the generated Rh metal nanoparticles. As a result, the active sites gradually decreased with photoirradiation time. On the other hands, it is very plausible that $TiO_{2-\delta}$ is easily generated on the anatase by photoirradiation and thus the amount of $TiO_{2-\delta}$ on the anatase does not decrease in the photodeposition. The abundance of $TiO_{2-\delta}$ on the anatase causes the constant appearance of Rh metal nanoparticles. In addition, it seems that the crystalline phase of TiO_2 contributes to the formation rate of $TiO_{2-\delta}$, which is now under discussion because it is difficult to analyze the formation rate of $TiO_{2-\delta}$ directly and accurately.

Conclusion

In the photodeposition process, the Rh metal nanoparticles with a uniform size appear on both anatase and rutile phase of TiO_2, and the appearance rate of Rh metal nanoparticles is constant on the anatase while it decreases with the photoirradiation time on the rutile. The behavior of reduction of Rh^{3+} ions to Rh^0 metals on the anatase is different from that on the rutile since the crystalline phase of TiO_2 has an effect on the rates of reduction of Rh^{3+} ions to Rh^0 metal nanoparticles on $TiO_{2-\delta}$.

Reference

(1) Kraeutler, B.; Bard, A. J. *J. Am. Chem. Soc.* **1978**, *100*, 4317.
(2) Herrmann, J. M.; Disdier, J.; Pichat, P. *J. Phys. Chem.* **1986**, *90*, 6028.
(3) Tanaka, K.; Harada, K.; Murata, S. *Sol. Energy* **1986**, *36*, 159.
(4) Maeda, K.; Teramura, K.; Lu, D.; Saito, N.; Inoue, Y.; Domen, K. *Angew. Chem. Int. Ed.* **2006**, *45*, 7806.
(5) Tsuji, I.; Kato, H.; Kobayashi, H.; Kudo, A. *J. Am. Chem. Soc.* **2004**, *126*, 13406.
(6) Caballero, A.; González-Elipe, A. R.; Fernández, A.; Herrmann, J. M.; Dexpert, H.; Villain, F. *J. Photochem. Photobiol., A* **1994**, *78*, 169.
(7) Teramura, K.; Okuoka, S.-i.; Yamazoe, S.; Kato, K.; Shishido, T.; Tanaka, T. *J. Phys. Chem. C* **2008**, *112*, 8495.
(8) Ohyama, J.; Teramura, K.; Okuoka, S.-i.; Yamazoe, S.; Kato, K.; Shishido, T.; Tanaka, T. *Langmuir* **2010**, *26*, 13907.
(9) Ohyama, J.; Yamamoto, A.; Teramura, K.; Shishido, T.; Tanaka, T. *ACS Catal.*, **2011**, 187.
(10) Li, Y.; Fan, Y.; Yang, H.; Xu, B.; Feng, L.; Yang, M.; Chen, Y. *Chem. Phys. Lett.* **2003**, *372*, 160.
(11) Wahlström, E.; Lopez, N.; Schaub, R.; Thostrup, P.; Rønnau, A.; Africh, C.; Lægsgaard, E.; Nørskov, J. K.; Besenbacher, F. *Phys. Rev. Lett.* **2003**, *90*, 026101.

(12) Min, B. K.; Wallace, W. T.; Santra, A. K.; Goodman,

D. W. *J. Phys. Chem. B* **2004**, *108*, 16339.